

Emergent stability in complex network dynamics

Received: 4 September 2022

Accepted: 7 March 2023

Published online: 20 April 2023

 Check for updates

Chandrakala Meena  , Chittaranjan Hens  , Suman Acharyya  ,
Simcha Haber , Stefano Boccaletti   & Baruch Barzel  

The stable functionality of networked systems is a hallmark of their natural ability to coordinate between their multiple interacting components. Yet, real-world networks often appear random and highly irregular, raising the question of what are the naturally emerging organizing principles of complex system stability. The answer is encoded within the system's stability matrix—the Jacobian—but is hard to retrieve, due to the scale and diversity of the relevant systems, their broad parameter space and their nonlinear interaction dynamics. Here we introduce the dynamic Jacobian ensemble, which allows us to systematically investigate the fixed-point dynamics of a range of relevant network-based models. Within this ensemble, we find that complex systems exhibit discrete stability classes. These range from asymptotically unstable (where stability is unattainable) to sensitive (where stability abides within a bounded range of system parameters). Alongside these two classes, we uncover a third asymptotically stable class in which a sufficiently large and heterogeneous network acquires a guaranteed stability, independent of its microscopic parameters and robust against external perturbation. Hence, in this ensemble, two of the most ubiquitous characteristics of real-world networks—scale and heterogeneity—emerge as natural organizing principles to ensure fixed-point stability in the face of changing environmental conditions.

The study of complex systems is often directed towards dramatic events, such as cascading failures^{1–5} or abrupt state transitions^{6–10}. In reality, however, these represent the exception rather than the rule. In fact, the truly intriguing phenomenon is that despite enduring constant perturbations and local obstructions, many systems continue to sustain reliably stable dynamics^{11–14}. This is achieved in the absence of a detailed design, as indeed, the dynamics of the majority of complex systems are mediated by random—often extremely heterogeneous—networks comprising a large number of interacting components, and

driven by a vast space of microscopic parameters. What then are the roots of this observed stability?

The answer lies in the system's linear stability matrix, namely, its Jacobian J , whose principal eigenvalue λ determines its response to perturbation^{15,16}. According to the linear stability theory, perturbations may either grow exponentially ($\text{Re}(\lambda) > 0$) capturing instability, or decay exponentially ($\text{Re}(\lambda) < 0$) if the system is stable. The challenge is that the structure of J remains elusive, given the scale, diversity and multiple parameters characterizing real-world complex systems.

¹Department of Mathematics, Bar-Ilan University, Ramat-Gan, Israel. ²Gonda Multidisciplinary Brain Research Center, Bar-Ilan University, Ramat-Gan, Israel. ³Chemical Engineering & Process Development, CSIR-National Chemical Laboratory, Pune, India. ⁴Indian Institute of Science Education and Research, Thiruvananthapuram, India. ⁵Physics and Applied Mathematics Unit, Indian Statistical Institute, Kolkata, India. ⁶Center for Computational Natural Sciences and Bioinformatics, International Institute of Information Technology, Gachibowli, Hyderabad, India. ⁷CNR—Institute of Complex Systems, Florence, Italy. ⁸Moscow Institute of Physics and Technology (National Research University), Moscow, Russian Federation. ⁹Universidad Rey Juan Carlos, Madrid, Spain. ¹⁰Network Science Institute, Northeastern University, Boston, MA, USA.  e-mail: meenachandrakala@gmail.com; baruchbarzel@gmail.com

To address this, we derive the dynamic Jacobian ensemble, showing that for a rather broad class of dynamics, stability is determined by a small set of analytically accessible parameters. We further show that this ensemble predicts an emergent stability, asymptotically robust in the thermodynamic limit ($N \rightarrow \infty$). Therefore, it offers precisely the desired natural design principles to ensure complex system stability^{17–19}.

Results

Fixed-point dynamics

Consider a complex system of N interacting components (nodes), whose dynamic activities $\mathbf{x}(t) = (x_1(t), \dots, x_N(t))^T$ are driven by pairwise interactions, potentially nonlinear. The system's fixed points \mathbf{x}_α capture static states, which—when unperturbed—remain independent of time. The dynamics in the vicinity of these fixed points can be examined through the system's response to small perturbations $\delta\mathbf{x}(t)$, which—in the linear regime—can be approximated by

$$\frac{d\delta\mathbf{x}}{dt} = J\delta\mathbf{x} + O(\delta\mathbf{x}^2). \quad (1)$$

Here J , an $N \times N$ matrix, represents the system's Jacobian around \mathbf{x}_α , which approximates—through a set of linear equations—the original nonlinear system's dynamics in the perturbative limit, that is, small activity changes $\mathbf{x}(t) = \mathbf{x}_\alpha + \delta\mathbf{x}(t)$. Hence, the spectral properties of J , particularly its principal eigenvalue λ , are crucial for characterizing the system's fixed-point behaviour.

Two factors shape J —the system's topology (that is, who interacts with whom) and its internal dynamics (namely, what is the nature of these interactions).

Topology

The first ingredient that impacts the structure of J is the network topology A , a binary matrix ($A_{ij} \in \{0, 1\}$, $A_{ii} = 0$), typically sparse and often highly heterogeneous²⁰. Designed to capture the linear response between i and j , the off-diagonal terms of J vanish if there is no direct i – j link, that is, $A_{ij} = 0 \Leftrightarrow J_{ij} = 0$ for all $i \neq j$. If, however, $A_{ij} = 1$, then the relevant term is assigned a weight W_{ij} that captures the strength of the linear dependence of i on j . Together, this leads to

$$J = (A - I) \circ W, \quad (2)$$

where the Hadamard product \circ represents element-by-element matrix multiplication and I is the $N \times N$ identity matrix. In equation (2), the network structure (A) determines the non-vanishing terms in J , and W determines their weights. The diagonal entries J_{ii} are introduced through the second term, $I \circ W$, where W_{ii} quantifies the self-linear dependence of $x_i(t)$.

Dynamics—the random matrix paradigm

To complete the construction of equation (2), we must assign all the weights W . In many of the traditional analyses, these unknown weights are extracted from two preselected probability densities, namely, $P_0(w)$ and $P_1(w)$, for the diagonal and off-diagonal terms, respectively. This gives rise to the Jacobian ensemble $\mathbb{E}(A, P_0, P_1)$, in which one first sets the topology A and then extracts weights from $P_0(w)$ and $P_1(w)$ (Fig. 1a–c).

As a classic example for this ensemble, we consider the construction²¹ in which A is an Erdős–Rényi (ER) network, the off-diagonal weights follow $W_{ij} \sim \mathcal{N}(0, \sigma^2)$, a zero-mean normal distribution, and the diagonal entries are uniformly set to $W_{ii} = 1$. Hence, the interaction strengths are potentially random, but the self-dynamics are driven by the system's intrinsic relaxation timescales, here normalized to unity. In the 'Random-matrix-based Jacobian constructions' section, we discuss more detailed constructions that have later built on this random matrix paradigm.

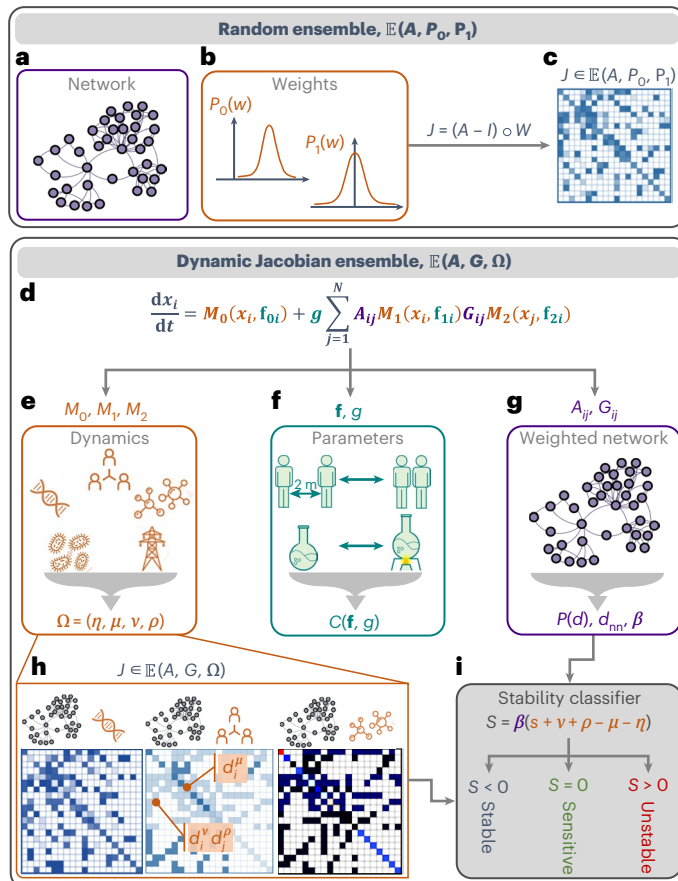


Fig. 1 | The dynamic Jacobian ensemble. To predict dynamic stability, we seek the system's stability matrix J . **a,b**, The classic approach is to structure/around the network topology A (**a**), with weights extracted from two distributions (**b**): $P_0(w)$ for the diagonal entries J_{ii} and $P_1(w)$ for the interactions strengths J_{ij} , where $i \neq j$. **c**, This results in $J \in \mathbb{E}(A, P_0, P_1)$, a random-matrix-based construction, whose stability is determined by structure A and random weights W . **d,e**, The dynamic ensemble (**d**) features emergent patterns that arise from the functional form of $M_q(x)$ (**e**; orange), capturing the system's ingrained dynamics, for example, social, biological or technological. We directly derive Ω (equations (4) and (5)) from these three functions. **f,g**, Microscopic parameters **f** and **g** (turquoise) that provide the specific rate constants for the dynamic processes mentioned in equation (3). For example, the infection rate in Epidemic (top) or the degradation rate in Biochemical (bottom). These parameters are tunable and may change following shifts in social behaviour (Epidemic) or temperature (Biochemical). Their impact on J is encapsulated within the coefficient $C(f, g)$ (equation (4)). **g**, Here A and G represent the weighted network (purple), expressed in/via the density function $P(d)$, the nearest-neighbour degree d_{nn} in equation (6) and β in equation (7). **h**, The resulting ensemble $J \in \mathbb{E}(A, G, \Omega)$ exhibits non-random scaling patterns. Similar to the random $\mathbb{E}(A, P_0, P_1)$, the non-vanishing terms correspond to the network links; however, in contrast to the random weights of $\mathbb{E}(A, P_0, P_1)$, here the weight of the i and j entry depends on d_i and d_j , respectively, as well as on Ω (orange captions). The result is a dynamic ensemble, in which identical networks (A and G) yield highly distinctive/matrices depending on $M_q(x)$, for example, Regulatory (left), Epidemic (centre) or Biochemical (right). **i**, Stability boils down to the classifier S in equation (9), whose value depends on degree heterogeneity (β ; purple) and Ω (orange terms), but not on the parameters **f** and **g**. Therefore, it provides a robust classification into stable (blue) or unstable (red) dynamics, asymptotically insensitive to changes in these parameters. Under $S = 0$, the system becomes sensitive (green), and stability is precisely driven by the parameters **f** and **g**.

The $\mathbb{E}(A, P_0, P_1)$ ensemble described above has two crucial shortcomings: (1) it provides no explicit guidelines on how to connect $P_0(w)$ and $P_1(w)$ with the system's specific nonlinear interactions;

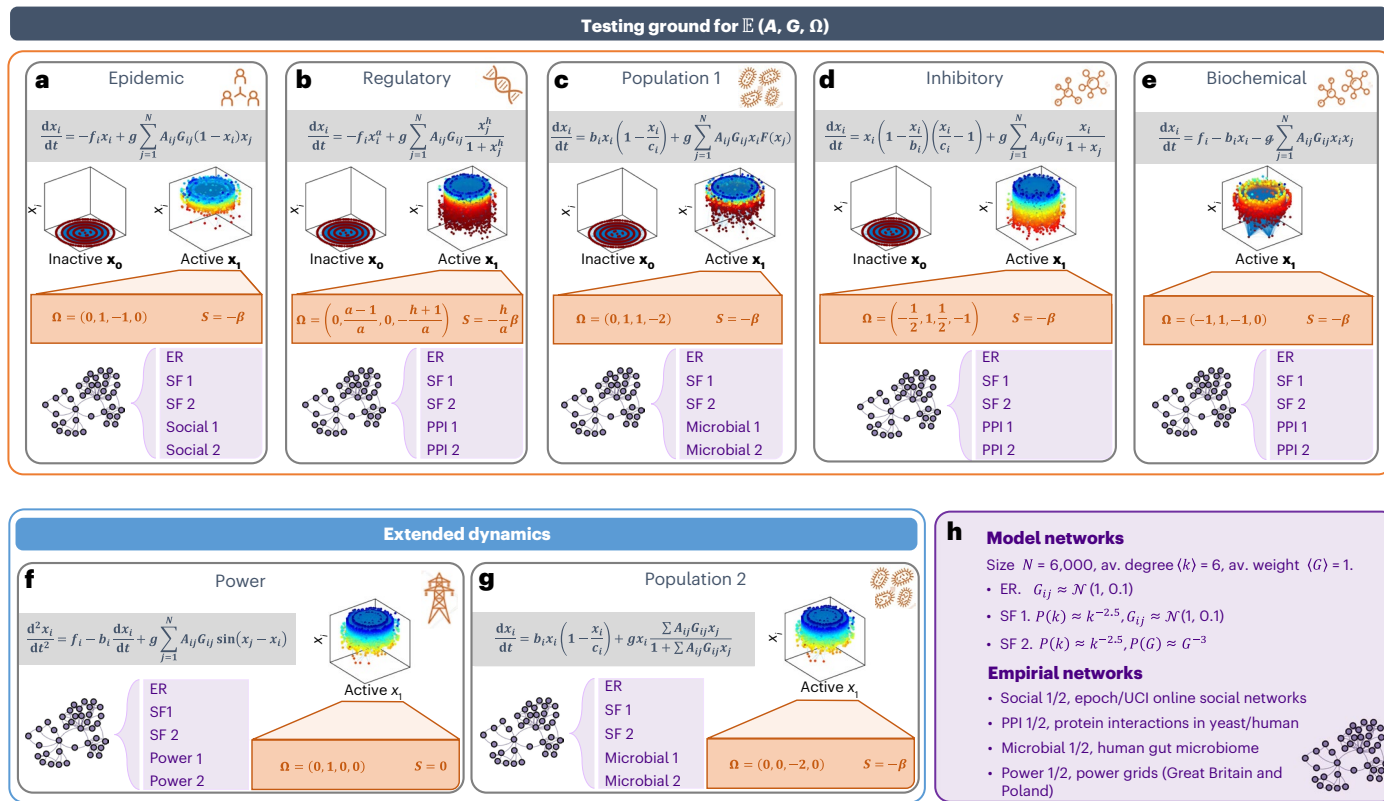


Fig. 2 | Testing ground for the $\mathbb{E}(A, G, \Omega)$ ensemble. We constructed different combinations of (weighted) networks A and G and dynamics $M_q(x)$ to examine our J ensemble. **a**, Epidemic: we implemented the susceptible–infected–susceptible dynamics (grey box) on a set of model and real-world networks (violet box). This system exhibits two potential fixed points (3D plots): inactive x_0 in which all the activities vanish (that is, healthy) and active x_1 in which all $x_i > 0$ (namely, pandemic). In this 3D visualization, the nodes $i = 1, \dots, N$ are laid out on the x - y plane and their fixed-point activity x_i is represented by colour (red, low; blue, high) and vertical displacement (z axis). Therefore, in x_0 , all the nodes are on the x - y plane ($z = 0$); in x_1 , they are distributed along $z > 0$ and range from red to blue. In each of these states, the system has a different set of exponents Ω and hence a different Jacobian J . Here we present Ω and S for the non-vanishing state x_1 (orange box). The remaining panels follow a similar format. **b**, Regulatory: subcellular dynamics following the Michaelis–Menten model. Here Ω and S depend on the model exponents a and h , respectively. **c**, Population 1: mutualistic dynamics between components of a population. **d**, Inhibitory: suppression dynamics, for example, between hosts and pathogens. **e**, Biochemical: protein–protein interactions modelled via mass-action kinetics. This system exhibits a single fixed point. **f**, Power: synchronization dynamics between components of a power system. **g**, Population 2: mutualistic population dynamics with non-additive interactions, namely, replacing the term $\sum_{j=1}^N A_{ij} G_{ij} M_2(x_j)$ in equation (3) by $M_2(\sum_{j=1}^N A_{ij} G_{ij} x_j)$. **h**, Our networks, including ER and scale-free networks, with both normally distributed and power-law-distributed weights, together with relevant empirical networks. Supplementary Section 7.4 provides a detailed description of all the networks. Together, we arrive at a set of 35 combinations of networks/dynamics on which we test our theoretical framework. Supplementary Section 4 provides a detailed analysis of all the dynamic models. Note that Population 2 (g) and Power (f) are not in the form of equation (3), and hence, they expand our testing ground beyond the bounds of our analytical framework (Supplementary Section 5).

interactions in, for example, in microbial communities. **d**, Inhibitory: suppression dynamics, for example, between hosts and pathogens. **e**, Biochemical: protein–protein interactions modelled via mass-action kinetics. This system exhibits a single fixed point. **f**, Power: synchronization dynamics between components of a power system. **g**, Population 2: mutualistic population dynamics with non-additive interactions, namely, replacing the term $\sum_{j=1}^N A_{ij} G_{ij} M_2(x_j)$ in equation (3) by $M_2(\sum_{j=1}^N A_{ij} G_{ij} x_j)$. **h**, Our networks, including ER and scale-free networks, with both normally distributed and power-law-distributed weights, together with relevant empirical networks. Supplementary Section 7.4 provides a detailed description of all the networks. Together, we arrive at a set of 35 combinations of networks/dynamics on which we test our theoretical framework. Supplementary Section 4 provides a detailed analysis of all the dynamic models. Note that Population 2 (g) and Power (f) are not in the form of equation (3), and hence, they expand our testing ground beyond the bounds of our analytical framework (Supplementary Section 5).

(2) by independently assigning A and W , it ignores the potential interplay between the network structure and dynamic weights of J . This stands in sharp contrast with the frequently observed fact that similar networks potentially exhibit profoundly distinct response patterns^{22–24}. How then do we appropriately assign weights W in equation (2) to capture this interplay between structure and dynamics?

The dynamic Jacobian ensemble. To construct predictive J matrices, we consider each system’s specific interaction mechanisms. For example, in epidemic dynamics, individuals interact through infection and recovery^{25–27}; in biological networks, proteins, genes and metabolites are linked through biochemical processes^{28–31}; and in population dynamics, species undergo competitive or symbiotic exchanges^{32–35}. Quite generally, these dynamic mechanisms can be represented by

$$\frac{dx_i}{dt} = M_0(x_i(t), \mathbf{f}_{0i}) + g \sum_{j=1}^N A_{ij} M_1(x_i(t), \mathbf{f}_{1i}) G_{ij} M_2(x_j(t), \mathbf{f}_{2j}), \quad (3)$$

a framework recently introduced to treat network dynamics²². Here $M_0(x_i, \mathbf{f}_{0i})$ captures the self-dynamics of all the nodes, and the

product function $M_1(x_i, \mathbf{f}_{1i}) \times M_2(x_j, \mathbf{f}_{2j})$ describes the i, j pairwise interaction. Each of these functions, $M_q(x, \mathbf{f}_{qi})$, where $q = 0, 1, 2$, is characterized by a set of parameters \mathbf{f}_{qi} , or collectively \mathbf{f} , capturing the rate constants that may be potentially distributed across the system’s components. Hence, the functional form of $M_q(x)$ is uniform throughout the network; yet, the specific rates and coefficients \mathbf{f} are node/link specific. In a similar fashion, the global interaction rate g increases/decreases the strength of all the interactions, whereas the specific i, j interaction strength is governed by the potentially diverse weight matrix G_{ij} . Together, equation (3) provides a generic template, allowing—by appropriately selecting $M_q(x)$ —to cover a range of frequently used models in social^{25,26}, biological^{28–32} and technological³⁶ systems (Fig. 2; the ‘Ingredients of $\mathbb{E}(A, G, \Omega)$ ’ section and Supplementary Section 1 provide an expanded discussion on equation (3)).

Dynamic Jacobians

As shown in Fig. 1h, to obtain J , we relinquish the random matrix construction $\mathbb{E}(A, P_0, P_1)$ and directly extract the Jacobian from equation (3). In Supplementary Section 2, we show that this leads to a currently unexplored matrix ensemble in which the Jacobian weights W

in equation (2) are strongly intertwined with the weighted topology A and G via

$$W_{ii} \sim C(\mathbf{f}, g) d_{nn}^\eta d_i^\mu \quad (4)$$

for the diagonal weights $J_{ii} = -W_{ii}$, and

$$W_{ij} \sim d_i^\nu G_{ij} d_j^\rho \quad (5)$$

for the off-diagonal weights $J_{ij} = A_{ij} W_{ij}$ ($i \neq j$). In equations (4) and (5), $d_i = \sum_{j=1}^N A_{ij} G_{ij}$ represents the weighted degree of node i , and

$$d_{nn} = \frac{1}{N} \sum_{i=1}^N \frac{1}{d_i} \sum_{j=1}^N A_{ij} G_{ij} d_j \quad (6)$$

represents the average weighted degree of a nearest-neighbour node⁷. Together, the two parameters d_i and d_{nn} capture the role of the weighted network topology (Fig. 1g). The four exponents $\Omega = (\eta, \mu, \nu, \rho)$ are determined by the dynamics, that is, the functions $M_q(x)$ and hence capture the role of the system's internal driving mechanisms (Fig. 1e). In the case of multiple fixed points, we have Ω_1, Ω_2 and so on—a potentially distinct exponent set for each fixed point. The analytical extraction of Ω from $M_q(x)$ is summarized in the 'Deriving the dynamic Jacobian ensemble' and 'Practical summary—calculating Ω ' sections. Finally, the coefficient $C(\mathbf{f}, g) > 0$ is governed by the rate constants \mathbf{f} and g in equation (3), which do not play a role in the scaling exponents Ω (Fig. 1f).

The resulting dynamic Jacobian in equations (4) and (5)—our first key result—is fundamentally distinct from the existing random-matrix-based constructions. On one hand, the network structure A continues to determine the non-zero entries, similar to the classic ensemble $\mathbb{E}(A, P_0, P_1)$. Also, the typical magnitude of the diagonal entries depends on the system's rates parameters through $C(\mathbf{f}, g)$, once again, analogous—although not identical—to the selection of $P_0(w)$ in the existing ensemble. However, the similarity ends there, as equations (4) and (5), in contrast to $\mathbb{E}(A, P_0, P_1)$ also capture the role of the system's nonlinearity. Specifically, they predict emergent patterns in the structure of J , which are rooted in the interplay between topology and dynamics: the degrees d_{nn}, d_i and d_j are extracted from the weighted network topology $A \circ G$ (Fig. 1g), whereas the scaling exponents Ω are derived from the dynamic functions $M_q(x)$ (Fig. 1e).

Therefore, we arrive at a new Jacobian ensemble $\mathbb{E}(A, G, \Omega)$, which—unlike the random $\mathbb{E}(A, P_0, P_1)$ —accounts for the effect of the system-specific nonlinear interaction dynamics. Consequently, in $\mathbb{E}(A, G, \Omega)$, identical networks may give rise to highly distinctive Jacobian matrices, depending on whether the interactions are, for example, social, biological or ecological, or even on the specific fixed point within each type of interaction. This is thanks to the unique set of exponents Ω , characterizing each of these systems/states (Fig. 1h).

Testing $\mathbb{E}(A, G, \Omega)$

To examine equations (4) and (5), we constructed a broad testing ground, including seven relevant dynamic models from different domains. Epidemic, the susceptible–infected–susceptible model^{25–27} for disease spreading; Regulatory, the Michaelis–Menten model²⁸ for gene regulation; Inhibitory, growth suppression in pathogen–host interactions³⁴; Biochemical, protein–protein interactions^{29–31} in sub-cellular networks; Populations 1 and 2, two models of mutualistic³² interactions in population dynamics; Power, load distribution in electric transmission networks. Applying each of these dynamics to five different model and relevant empirical networks, we arrive at a total of 35 combinations of networks/dynamics, on which we test our predicted ensemble (Supplementary Sections 4 and 7 provide a detailed description of all the models/networks and Supplementary Section 5 analyzes the additional dynamics).

In Fig. 2, we present—for each system—the dynamic equation (blue) and a list of relevant networks on which it was tested (violet). In some cases, the system features several fixed points, for example, Epidemic (Fig. 2a) exhibits a healthy state (inactive \mathbf{x}_0) and a pandemic state (active \mathbf{x}_1). These states are presented using a three-dimensional (3D) visualization. The network is laid out on the x – y plane, and the activities x_i of all the nodes are captured by the vertical z -axis displacement. Hence, under \mathbf{x}_0 , all the nodes remain on the x – y plane ($z = 0$), whereas in the active state \mathbf{x}_1 , all of them have $x_i > 0$. Finally, we display our predicted dynamic exponents $\Omega = (\eta, \mu, \nu, \rho)$ for each system around its active state (orange) (Supplementary Section 4 provides the derivation of Ω for inactive states).

Perturbing the system around its active fixed point, we constructed the Jacobian matrix J for each of our 35 systems (Supplementary Section 7.2). In Fig. 3, we find that, indeed, the diagonal (W_{ii}) and off-diagonal (W_{ij}) weights of our numerically obtained J (blue symbols) follow the predicted scaling of equations (4) and (5) (orange solid lines). For example, in Epidemic, we predict $\mu = 1$, whereas for Regulatory, we have $\mu = 0$, both scaling relationships clearly evident in Fig. 3b,d. This means that independently extracting all the diagonal terms from $P_0(w)$, as in $\mathbb{E}(A, P_0, P_1)$, misses the distinct patterns that arise from the nonlinear Epidemic/Regulatory dynamics. Similarly, the off-diagonal terms are proportional to $d_i^{-1} G_{ij} d_j^0$ in Epidemic (Fig. 3c) and $d_i^0 G_{ij} d_j^{-2}$ in Regulatory (Fig. 3e)—once again, in striking agreement with our theoretical predictions (orange solid lines). And yet, they are in stark contrast with the random construction $\mathbb{E}(A, P_0, P_1)$, where W_{ij} are blindly extracted from $P_1(w)$.

Our analysis further predicts that Ω depends only on $M_q(x)$, thus independent of network structure A , weights G or coefficients \mathbf{f} and g . We examine this in Fig. 3, by testing each of our dynamics on a diverse set of networks, with different degree/weight distributions. As predicted, we find that η, μ, ν and ρ are, indeed, universal, conserved across our diverse model (ER, scale-free 1 (SF 1) and scale-free 2 (SF 2)) and relevant empirical (Social 1, Social 2, PPI 1, PPI 2 and so on) networks. Hence, Ω captures the intrinsic—and most crucially, currently, overlooked—contribution of the nonlinear dynamics to the structure of J .

Together, our derivation demonstrates that (1) actual J matrices are fundamentally distinct from the commonly used random ensembles; (2) contrary to these ensembles, they feature non-random scaling patterns in which topology (d_{nn}, d_i, d_j) and dynamics (Ω) are deeply intertwined; (3) these patterns can be analytically traced to the system's dynamics $M_q(x)$ through equations (4) and (5), giving rise to our new dynamic Jacobian ensemble $\mathbb{E}(A, G, \Omega)$. Next, we use $\mathbb{E}(A, G, \Omega)$ to derive the conditions for the dynamic stability of equation (3).

Dynamic stability. The dynamic stability around a given fixed point is governed by the principal eigenvalue λ of J , requiring that $\text{Re}(\lambda) < 0$. To obtain λ , let us first focus on the role of the network topology A and G . The ingredients of $J \in \mathbb{E}(A, G, \Omega)$, as expressed in equations (4) and (5), suggest that λ is strongly linked to the network's weighted degree density function $P(d)$. This is directly indicated through the dependence on d_i and d_j , but also indirectly through the nearest-neighbour degree d_{nn} , whose magnitude depends on the system's degree heterogeneity³⁷. For instance, in a randomly wired network, we have $d_{nn} = \langle d^2 \rangle / \langle d \rangle$ (refs. 7,38), where the second moment $\langle d^2 \rangle$ increases with the variance of $P(d)$ and consequently with the heterogeneity of A and G . In case $P(d)$ is fat tailed, we have³⁷

$$d_{nn} \sim N^\beta, \quad (7)$$

an asymptotic divergence with system size. Hence, β helps characterize the network's degree heterogeneity, following $\beta = 0$ for homogeneous networks in which $P(d)$ is concentrated around its mean, and $\beta > 0$ for heterogeneous A and G where the variance is unbounded.

The remaining ingredients in equations (4) and (5) that may impact λ are $\Omega = (\eta, \mu, \nu, \rho)$ and $C(\mathbf{f}, g)$. Combining all the three contributions

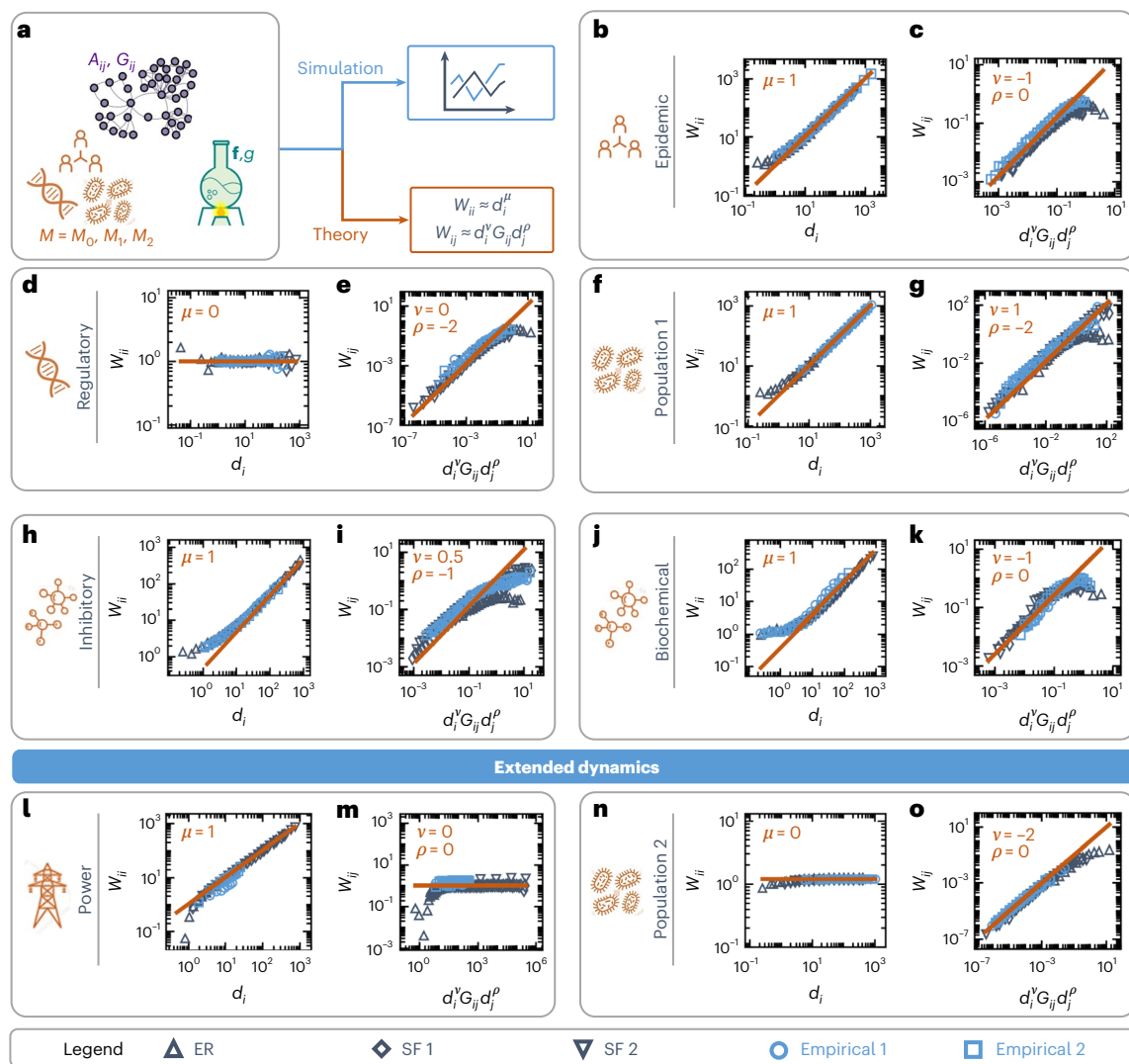


Fig. 3 | Emergent patterns in the dynamic ensemble $E(A, G, \Omega)$. We implemented our seven dynamic models on relevant model and empirical networks (Fig. 2); the legend is shown at the bottom. Perturbing all the nodes around their numerically obtained fixed point (x_i), we constructed the Jacobian. **a**, Numerical simulations incorporate the full complexity of equation (3): weighted network (purple), diverse parameters (turquoise) and nonlinear mechanisms (orange). This provides actual Jacobian matrices, obtained from numerical runs of the nonlinear network models (Simulation; blue, top). We compare our simulation results with our predictions in equations (4) and (5) (Theory; orange, bottom). **b**, Diagonal weights W_{ii} versus d_i as obtained from Epidemic dynamics (symbols). We observe our predicted scaling (equation (4)) with $\mu = 1$ (orange solid line). The scaling is independent of A and G , consistently observed in all our model/empirical networks—*intrinsic* to the Epidemic dynamics, as predicted. **c**, Off-diagonal weights W_{ij} versus our theoretical prediction in equation (5) with $v = -1, \rho = 0$ (symbols). Once again, we observe

perfect agreement between simulation (blue symbols) and theory (orange solid line). We also include two relevant empirical networks, namely, Social 1 and Social 2 (light-blue circles/squares), capturing online social dynamics.

d,e, Similar results are observed under Regulatory ($\mu = v = 0, \rho = -2$) on both model and empirical networks (PPI1 (d) and PPI2 (e)). **f,g**, Population 1 dynamics ($\mu = v = 1, \rho = -2$; empirical networks, Microbial1 (f) and Microbial2 (g)). **h,i**, Inhibitory dynamics ($\mu = 1, v = 1/2, \rho = -1$; empirical networks, PPI1 (h) and PPI2 (i)). **j,k**, Biochemical dynamics ($\mu = 1, v = -1, \rho = 0$; empirical networks, PPI1 (j) and PPI2 (k)). **l,m**, Power dynamics ($\mu = 1, v = \rho = 0$; empirical networks, Power 1 (l) and Power 2 (m)). **n,o**, Population 2 dynamics ($\mu = 0, v = -2, \rho = 0$; empirical networks, Microbial 1 (n) and Microbial 2 (o)). In all these systems, we find that the real Jacobian matrices (blue symbols) are well approximated by our theoretically predicted scaling laws (orange solid lines). Data in all the panels are logarithmically binned⁴². Supplementary Section 7 provides details on the numerical calculation of J , log-binning and all network data.

(Supplementary Section 3), we show that in $E(A, G, \Omega)$, the principal eigenvalue asymptotically follows

$$\text{Re}(\lambda) \sim N^Q \left(1 - \frac{C(\mathbf{f}, \mathbf{g})}{N^S} \right), \quad (8)$$

where $Q = \beta(1 + v + \rho - \eta/2)$ and

$$S = \beta(s + v + \rho - \mu - \eta). \quad (9)$$

In equation (9), the parameter S depends on the sign of the interactions, and $S = 1$ under cooperative interactions (positive J_{ij}), such as in Epidemic or Regulatory, and $s = 0$ if the interactions are adversarial (negative J_{ij}), for example, Inhibitory or Biochemical.

Equations (8) and (9)—our second key result—uncover the asymptotic behaviour of λ in the limit of a large complex system $N \rightarrow \infty$. Contrary to $E(A, P_0, P_1)$, in which λ is fully determined by A and G , here the exponents S and Q also depend on the dynamics via Ω . Most importantly, these equations have crucial implications regarding the

system's fixed-point stability, giving rise to three potential stability classes, uniquely predicted within our dynamic ensemble (Fig. 1i).

Asymptotic instability. In case S in equation (8) is positive ($S > 0$; Fig. 1i, red), we have, for sufficiently large N , $\text{Re}(\lambda) \sim N_Q > 0$. Therefore, as the system size N increases, such states inevitably become unstable. Asymptotic stability ($S < 0$; Fig. 1i, blue): for $S < 0$, we have $N^\delta \rightarrow 0$, the right-hand side of equation (8) is dominated by the negative term, and hence, $\text{Re}(\lambda) < 0$. Consequently, here as $N \rightarrow \infty$, stability becomes unconditionally guaranteed. Sensitive stability ($S = 0$; Fig. 1i, green): under $S = 0$, the system lacks an asymptotic behaviour, and therefore, its stability depends on $C(f, g)$ (equation (8)). If $C(f, g) > 1$, the system is stable; otherwise, it becomes unstable. Hence, in this class, stability is not driven by the system size N , but rather by the coefficient $C(f, g)$ and consequently by the rate parameters f and g in equation (3).

Stability classifier

The stability classifier S in equation (9) helps group all $J \in \mathbb{E}(A, G, \Omega)$ into distinct stability classes. It achieves this by identifying the relevant topological (β) and dynamic (Ω) control parameters that help analytically predict the stability of any system within the form of equation (3). We can, therefore, use S to predict a priori whether a specific combination of topology and dynamics will exhibit stable functionality or not.

To examine the predictive power of S , we tested it extensively against a diverse set of complex networks. In particular, we used our model and empirical networks to extract 7,387 Jacobian matrices from the $\mathbb{E}(A, G, \Omega)$ ensemble, with different sets of η, μ, ν and ρ . In Fig. 4a, we show the principal eigenvalue $\text{Re}(\lambda)$ versus S for the entire set of 7,387 Jacobian samples. As predicted, we find that parameter S sharply splits the sample into three classes. The asymptotically unstable class (Fig. 4a, red, top right) has $S > 0$ and consequently also $\text{Re}(\lambda) > 0$, a guaranteed instability. The asymptotically stable class (Fig. 4a, blue, bottom left) is observed for $S < 0$, and has, in all cases $\text{Re}(\lambda) < 0$, that is, stable dynamics. Finally, for $S = 0$, we observe sensitive stability, with $\text{Re}(\lambda)$ having no asymptotic behaviour, either positive or negative (Fig. 4a, green). A small fraction (~8%) of our sampled J

matrices were inaccurately classified by S (Fig. 4a, grey), an expected consequence of the approximate nature of the derivation of S (Supplementary Section 3).

Ingredients of dynamic stability. The parameter S in equation (9) reduces the dynamic stability of equation (3) into five relevant exponents. The first four ($\Omega = (\eta, \mu, \nu, \rho)$) are determined by the system's intrinsic dynamics $M_q(x)$, around each of its fixed points. The remaining exponent in equation (9), β , is independent of the dynamics, solely determined by A and G , specifically by their weighted degree density function $P(d)$, via equation (7). Therefore, together, S captures the roles of both topology and dynamics, whose interplay determines the system's stability class around a specific fixed point—stable, unstable or sensitive.

The only remaining factor in equation (8) is the coefficient $C(f, g)$, whose value is driven by rate parameters f and g of equation (3). Yet, as our analysis indicates, this factor is sidelined when $N \rightarrow \infty$ under $S \neq 0$. We interpret this to mean that under asymptotic stability or instability, the system's countless microscopic parameters turn irrelevant, and the stable/unstable fixed points of equation (3) become ingrained into the system's intrinsic dynamics, that is, the functional form of $M_q(x)$ (the 'Ingredients of $\mathbb{E}(A, G, \Omega)$ ' section and Supplementary Section 1 provide an expanded discussion on this distinction).

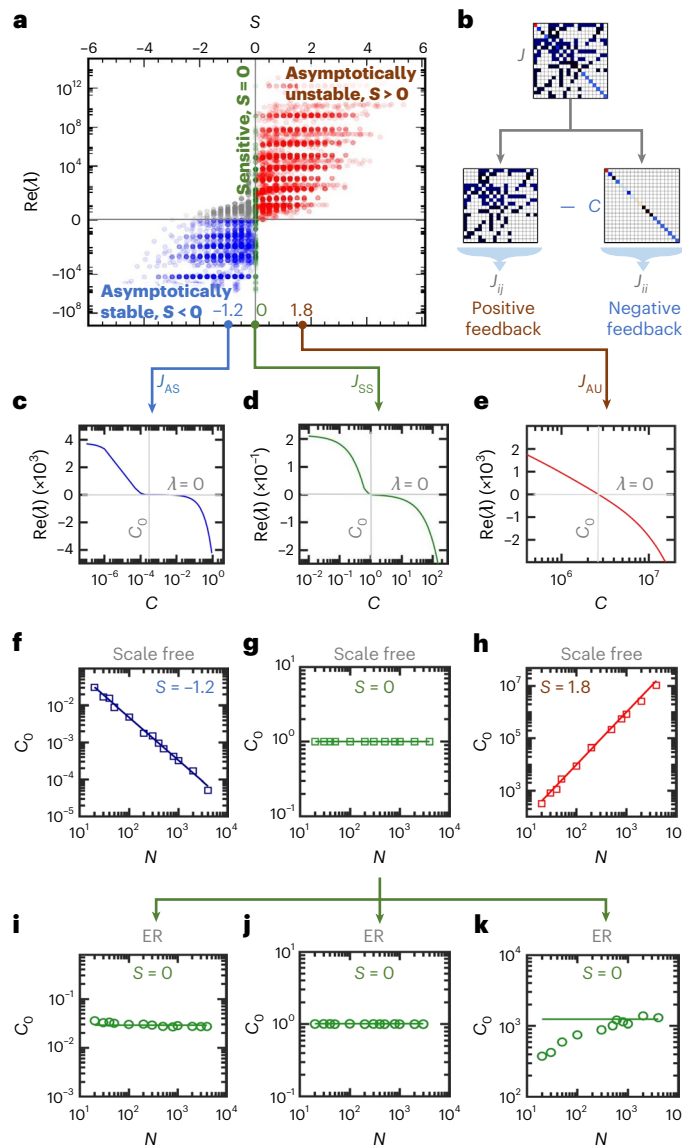


Fig. 4 | Three classes of dynamic stability. We extracted 7,387 Jacobian matrices from the $\mathbb{E}(A, G, \Omega)$ ensemble, using combinations of model/empirical networks with different dynamic exponents Ω . For each J , we calculated the principal eigenvalue λ and stability classifier S in equation (9). **a**, $\text{Re}(\lambda)$ versus S for all 7,387 matrices. We observe the three predicted classes: asymptotically unstable (red) in which $S > 0$ and hence, as predicted, we also have $\text{Re}(\lambda) > 0$; sensitively stable (green), where $S = 0$ and $\text{Re}(\lambda)$ can both be positive or negative; asymptotically stable (blue), where $S < 0$ and therefore $\text{Re}(\lambda) < 0$. Our classification showed ~4% inaccuracy on binary networks, ~5% on weighted networks and ~15% on weighted/negative networks—a total discrepancy of ~8% (grey dots) over the entire ensemble. **b**, Value of λ emerges from the competition between the off-diagonal terms of J , representing positive feedback, and the strength of the diagonal terms J_{ii} (negative feedback). Therefore, one can force a system towards stability ($\text{Re}(\lambda) < 0$) by increasing the coefficient C in equation (4). **c–e**, Taking three specific matrices, we plot $\text{Re}(\lambda)$ versus C , seeking the critical C_0 , in which $\text{Re}(\lambda)$ becomes negative (grey lines). This represents the critical C above which stability is ensured. **f**, For the stable J_{AS} ($S = -1.2$), we find that C_0 decreases with N (squares), capturing the asymptotic stability in which as $N \rightarrow \infty$, stability is sustained even under arbitrarily small C . The theoretical scaling predicted in equation (10) is also shown (solid line; slope, -1.2). **g**, For J_{SS} , we have $S = 0$, the critical C_0 is independent of N , and hence, the system's stability can be affected by finite changes to its dynamic parameters. **h**, Asymptotically unstable J_{AU} ($S = 1.8$) has $C_0 \rightarrow \infty$ in the limit of large N , in perfect agreement with equation (10) (solid line). Here no matter how large C is, the fixed point associated with J_{AU} is always unstable. **i–k**, For a homogeneous $P(d)$, for example, ER, β vanishes and hence $S = 0$ in equation (9). Under these conditions, regardless of Ω , the system is always sensitively stable, and therefore, C_0 does not scale with N . This demonstrates the role of degree heterogeneity for ensuring stability in the face of changing environmental conditions.

To gain a deeper insight, consider, for example, the factors that drive a system towards the loss of stability. Most often, such events result from external stress or changes in environmental conditions⁷. Such forces impact the system by perturbing its dynamic parameters, for example, changing the rates of specific processes. Seldom, however, do these environmental perturbations affect the system's built-in interaction mechanisms. Indeed, these mechanisms are ingrained in the physics of the interacting components, and therefore, they are unaffected by external conditions. Hence, asymptotic stability ($S < 0$, $N \rightarrow \infty$) depicts robust dynamic states that are insensitive to changes in environmental conditions.

Role of degree heterogeneity

The dependence of S in equation (9) on β highlights the crucial role that $P(d)$ plays in dynamic stability. To understand this, consider a homogeneous network, such as ER with randomly assigned weights. Here $P(d)$ follows a Poisson distribution, having $\beta = 0$. Under these conditions, we have $S = 0$ in equation (9); the system has no defined asymptotic behaviour, and hence, it is sensitively stable—that is, its stability depends on model parameters via $C(f, g)$. Hence, our predicted asymptotically stable/unstable classes depend on $\beta > 0$, indicating that they emerge as a direct consequence of degree heterogeneity. This suggests that a fat-tailed $P(d)$, indeed—among the defining features of many real-world complex systems²⁰—serves as a dynamically stabilizing structure, locking-in specific fixed points, in the face of a persistently fluctuating environment.

To further uncover the roots of asymptotic stability/instability, we again consider the principal eigenvalue λ of $\mathbb{E}(A, G, \Omega)$ (equation (8)). Its structure portrays stability as a balance between the positive (destabilizing) effect mediated by network interactions versus the negative (stabilizing) feedback driven by parameter $C(f, g)$ in the diagonal of J (equation (4)) (Fig. 4b). It is, therefore, natural to enhance the stability by increasing $C(f, g)$, which, in effect, translates to strengthening each node's intrinsic self-regulation. Equation (8) predicts that J becomes stable if $C(f, g)$ exceeds a critical value of

$$C_0 \sim N^S, \quad (10)$$

beyond which λ turns negative. For asymptotically stable states ($S < 0$), we have, for sufficiently large N , $C_0 \rightarrow 0$ —a guaranteed stability even under arbitrarily small $C(f, g)$. In contrast, for asymptotically unstable states ($S > 0$), we have $C_0 \rightarrow \infty$, and hence, such systems are impossible to stabilize even under extremely large $C(f, g)$. We emphasize that $C(f, g)$ is the only component in equation (8) that is dependent on the system's tunable parameters and therefore has an unbounded range of C values under which the system remains stable (or unstable) guarantees that λ is, indeed, unaffected by parameter perturbation, such as, changing environmental conditions.

To test equation (10), in Fig. 4c–k, we extract a set of three specific J matrices from $\mathbb{E}(A, G, \Omega)$, representing systems from our three stability classes: J_{AS} , asymptotically stable with $\Omega = (2, 2, 2, -1)$; J_{SS} , sensitively stable with $\Omega = (0, -1, -2, 0)$; J_{AU} , asymptotically unstable with $\Omega = (1, -2, -1, 2)$. For each of these systems, we plot C_0 versus N , capturing the level of negative feedback required to ensure system's stability. Under ER ($\beta = 0$; Fig. 4i–k), we do not observe a defined asymptotic behaviour. The critical C_0 value does not scale with N , indicating that sufficient perturbation to the model parameters can, indeed, affect the stability of J .

In contrast, the same J matrices on SF 1 ($\beta = 0.6$) exhibit a clear asymptotic behaviour, congruent with equation (10). For J_{AS} , we have $C_0 \approx N^{-1.2}$, whereas under J_{AU} , we observe $C_0 \approx N^{1.8}$ (Fig. 4f–h, squares), precisely as predicted (solid lines). Finally, in J_{SS} , for which $S = 0$, the system again lacks an asymptotic behaviour and therefore can be stabilized (or destabilized) under finite C_0 , independent of system size N (Fig. 4g).

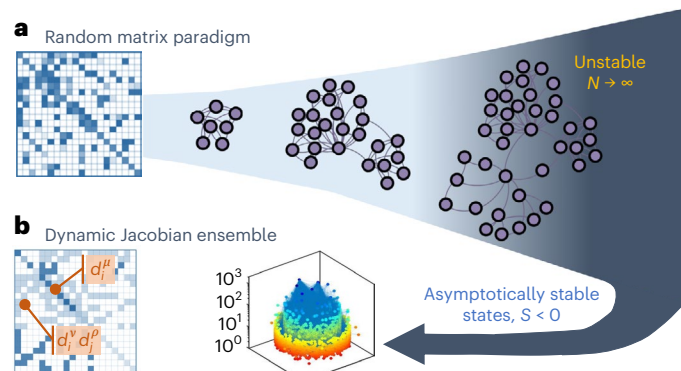


Fig. 5 | Will a large complex system be stable? This question, first posed by May in 1972 (ref. 21), captures a long-standing challenge, fuelled by the seeming contradiction between theory and practice. **a**, Although empirical reality answers with an astounding yes, May's mathematical analysis, based on random matrix theory, suggested the contrary: large systems are inevitably unstable, giving rise to the well-known diversity–stability debate. Here the series of growing networks (left to right) become increasingly unstable as we drift towards $N \rightarrow \infty$. In subsequent works, it became clear that real-world complex systems are not random. Rather, they incorporate unique structural^{13–15} and dynamic^{18,19,46} constraints—or organizing principles—that can potentially enhance stability. **b**, Our dynamic Jacobian ensemble offers such organizing principles, which emerge fairly naturally in a variety of real-world systems (Fig. 2). This is expressed through the built-in scaling patterns in J (orange), which, in turn, predict a broad class of asymptotically stable dynamic states (middle). In this class ($S < 0$), the system size plays a stabilizing rather than a destabilizing role. Consequently, we arrive at fairly broad conditions where May's original question receives a clear answer: large complex systems not only can but often must be stable.

Together, equation (10) helps us link the scale N of a complex system with its observed stability. As opposed to the random matrix viewpoint of $\mathbb{E}(A, P_0, P_1)$, in which N has a destabilizing effect and hence large systems become unstable²¹, our dynamic ensemble uncovers broad conditions where the contrary is true, and $N \rightarrow \infty$, is, in fact, what anchors the system's stability (Fig. 5). Next, we return to our testing ground of dynamical systems (Fig. 2) to examine this asymptotic stability, not just on artificially constructed J but under the full nonlinear setting of equation (3).

Emergent stability

The stabilizing/destabilizing effect of N and $P(d)$ is especially relevant if equation (3) exhibits multiple fixed points, for example, an undesirable \mathbf{x}_0 and a desirable \mathbf{x}_1 . In $\mathbb{E}(A, G, \Omega)$, these two states can be potentially characterized by two different exponent sets Ω_0 and Ω_1 and consequently a different stability profile. For example, if \mathbf{x}_0 is asymptotically unstable ($S > 0$) and \mathbf{x}_1 is asymptotically stable ($S < 0$), then a large ($N \rightarrow \infty$) heterogeneous ($P(d)$ fat-tailed) network will firmly reside only in \mathbf{x}_1 , unaffected by perturbation to f or g .

To observe this, we return to our testing ground of Fig. 2, and we focus on dynamic models that have multiple fixed points. This includes Regulatory, Epidemic and Inhibitory, each of which exhibits—on top of its active state \mathbf{x}_1 in which all $x_i > 0$ —an inactive state $\mathbf{x}_0 = (0, \dots, 0)^T$, where all the activities vanish (Population 1 and Population 2 also exhibit an inactive \mathbf{x}_0 ; however, it is never stable; Supplementary Section 4.3).

First, we simulate Regulatory on an ER network, and vary the model's two parameters: the individual node degradation rate f , and the global interaction strength g . We find that when the average $\langle f \rangle$ is large or, alternatively, when g is small, the system resides in \mathbf{x}_0 , whereas in the opposite limit, it favours \mathbf{x}_1 (Fig. 6c–e, diamonds). This is precisely the sensitive stability in which the system's fixed-point behaviour is driven by its microscopic parameters. Repeating the same experiment

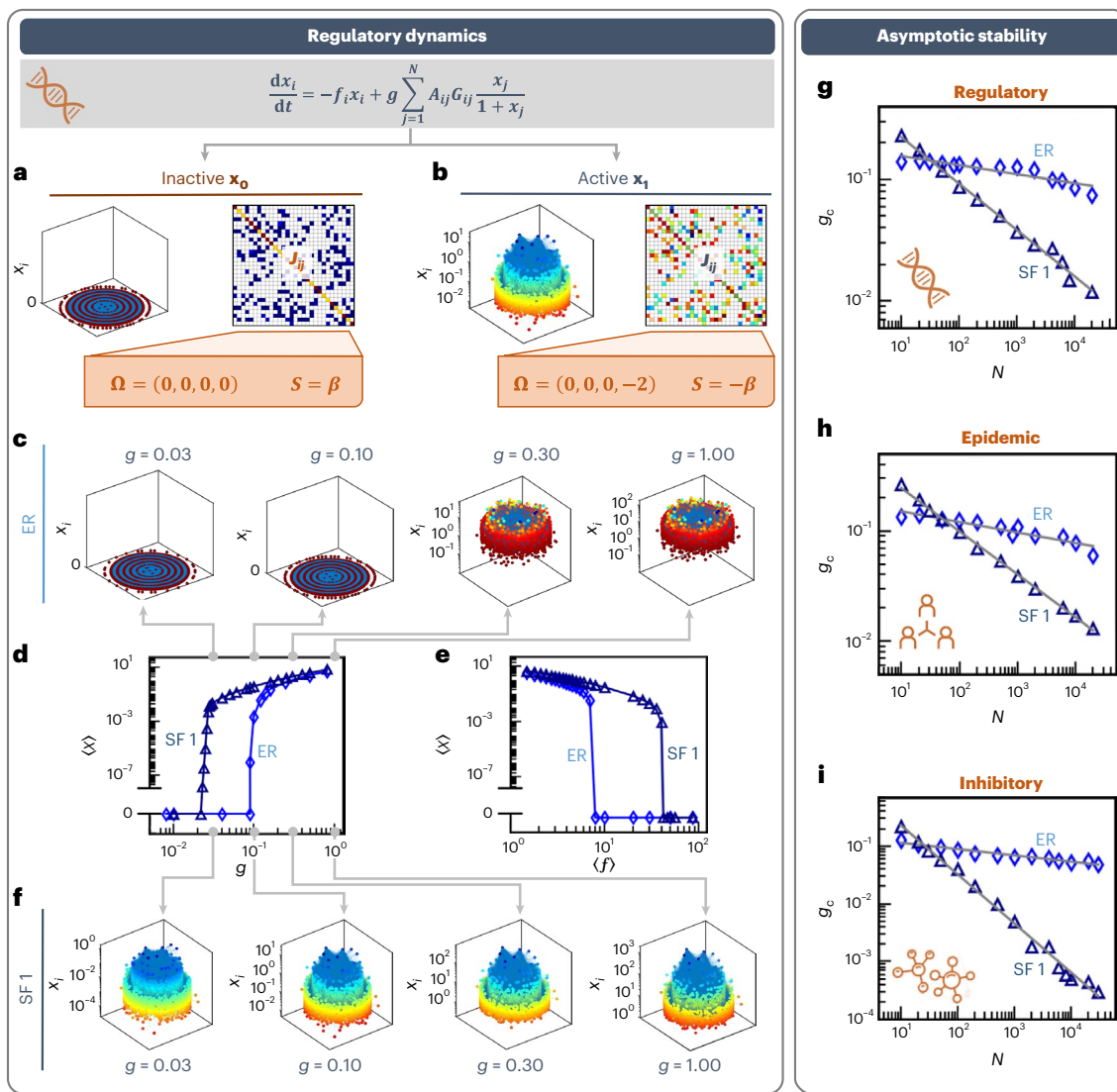


Fig. 6 | Emergent stability in large heterogeneous networks. **a,b,** Regulatory dynamics exhibit two fixed points (3D plots), each with its own $J \in \mathbb{E}(A, G, \Omega)$ (right). Inactive \mathbf{x}_0 (**a**) has $\Omega = (0, 0, 0, 0)$ and $S = \beta > 0$, and hence, it is asymptotically unstable. Active \mathbf{x}_1 (**b**) has a different J , with $\Omega = (0, 0, 0, -2)$ and $S = -\beta < 0$ (asymptotically stable). **c**, State of Regulatory as obtained from numerical simulations on our ER network under varying g . The system transitions from \mathbf{x}_1 (right) to \mathbf{x}_0 (left) under small g . This represents sensitive stability, as indeed predicted for ER, in which parameters (here g) affect the state of the system. **d**, To systematically examine this, we plot the mean activity $\langle \mathbf{x} \rangle$ versus g as obtained for ER (diamonds) and SF1 (triangles). Both systems exhibit a critical g_c , below which \mathbf{x}_1 becomes unstable and the system transitions to \mathbf{x}_0 . The crucial point is, however, that owing to its heterogeneity, SF1 exhibits an increased robustness against g variations, with g_c being an order of magnitude lower than that observed for ER. **e**, $\langle \mathbf{x} \rangle$ versus f shows a similar behaviour (here increasing

f) causes the system to collapse to \mathbf{x}_0). **f**, State of SF1 under the same four conditions shown in **c**. As predicted, SF1 remains at \mathbf{x}_1 even when ER has already collapsed to \mathbf{x}_0 . **g**, The g_c value versus system size N as obtained from numerically simulating Regulatory dynamics. For ER, we observe $g_c \approx \text{constant}$ (diamonds); hence, there is a typical g_c , below which the system transitions to \mathbf{x}_0 . Consequently, \mathbf{x}_1 can be destabilized via parameter perturbation. Note that although N spans over four orders of magnitude, g_c varies by a mere 40%. In contrast, for SF1, we find that g_c exhibits negative scaling with N , approaching $g_c \rightarrow 0$ in the limit $N \rightarrow \infty$. This precisely captures the predicted asymptotic stability, in which a sufficiently large and heterogeneous network is guaranteed to stably reside in \mathbf{x}_1 even under arbitrarily small g (or large f). **h,i**, Repeating this experiment for Epidemic (**h**) and Inhibitory (**i**), we continue to observe our predicted asymptotic stability: under SF1, we have $g_c \rightarrow 0$ as $N \rightarrow \infty$, whereas under ER, g_c is (almost) independent of N .

on SF1, we observe that \mathbf{x}_1 is sustained for a broader range of f and g ; hence, SF1 is comparably insensitive to changes in these parameters (Fig. 6d-f, triangles). This robustness is a direct outcome of our classifier: \mathbf{x}_0 has $\Omega_0 = (0, 0, 0, 0)$, which in equation (9) predicts $S = \beta > 0$, whereas \mathbf{x}_1 has $\Omega_1 = (0, 0, 0, -2)$ and hence $S = -\beta < 0$. Therefore, on a large ($N \rightarrow \infty$) scale-free ($\beta > 0$) network, \mathbf{x}_0 becomes asymptotically unstable, and the system is forced to reside in the asymptotically stable \mathbf{x}_1 .

To systematically observe this, we seek the critical global weight g_c , below which \mathbf{x}_1 becomes unstable, and the system transitions to \mathbf{x}_0 . Varying the system size N over four orders of magnitude, from 10 to

2×10^4 , we observe first hand the asymptotic stability of \mathbf{x}_1 : while under ER, g_c is almost independent of N (Fig. 6g, diamonds), in SF1, it scales negatively with system size, approaching $g_c \rightarrow 0$ in the limit $N \rightarrow \infty$ (triangles). Hence, as predicted, the \mathbf{x}_1 state of SF1 remains stable even under arbitrarily small g_c , a stability entrenched by system size. This reconfirms equation (10), but this time, not on theoretically constructed J from $\mathbb{E}(A, G, \Omega)$ (Fig. 4f-k), but rather on the actual numerically simulated dynamics of equation (3). Similar stability patterns are also observed in Epidemic and Inhibitory (Fig. 6h,i and Supplementary Sections 4.1 and 4.5).

Role of hub nodes

We, therefore, observe a qualitative difference between homogeneous and fat-tailed $P(d)$, in which degree heterogeneity can potentially afford the network a guaranteed stability that is asymptotically independent of microscopic parameters. This phenomenon is rooted in the dominance of hub nodes, whose dynamic behaviour forces the entire system towards stability/instability. In this sense, one can think of our classifier S as a mathematical tool to precisely predict what will be the dynamic role of the hubs—whether the hubs serve as stabilizers ($S < 0$), destabilizers ($S > 0$) or neither ($S = 0$).

Discussion and outlook

The linear stability matrix/carries crucial information on the dynamic behaviour of complex systems. Here we exposed distinct patterns in the structure of/that arise from the nature of the system's interaction dynamics. These patterns are expressed through the four dynamic exponents $\Omega = (\eta, \mu, \nu, \rho)$, which we analytically link to the system's dynamic functions $M_q(x)$, independent of the weighted network topology A, G or parameters f, g . We interpret this to mean that Ω is hard-wired into the system's innate interaction dynamics, determined by the dynamic model, for example, Epidemic or Regulatory, but not by the specific model parameters or the system's underlying connectivity patterns. Therefore, our predicted Jacobian ensemble in equations (4) and (5), as well as its associated stability classifier S in equation (9), capture highly robust and distinctive characteristics of the system's dynamics, which cannot be perturbed or otherwise affected by shifting environmental conditions.

Graph spectral analysis represents a central mathematical tool to translate network structure into dynamic predictions^{39–41}. A network's spectrum, namely, its set of eigenvalues and eigenvectors, captures information on its dynamic timescales, potential states and—in the present context—its dynamic stability. Most often, spectral analysis is applied to the network topology, that is, we seek the graph's eigenvalues, thus overlooking information on the nonlinear dynamics that occur on that graph. As an alternative, our $\mathbb{E}(A, G, \Omega)$ ensemble suggests to apply spectral analysis, not to topology A (or weighted $A \circ G$), but rather to J , which—thanks to Ω —preserves the information of both structure and dynamics.

Strictly speaking, our analysis covers the Barzel–Barabási family of equations (equation (3)). Having said that, it also shows strong numerical indications for broader relevance beyond this family (the 'Generality and limitations of the $\mathbb{E}(A, G, \Omega)$ ensemble' section and Supplementary Section 5). Most importantly, it motivates a departure from the decades-old random matrix paradigm ($\mathbb{E}(A, P_0, P_1)$) by showing that real-world Jacobians are anything but random. Hence, although the analytically predictable scaling patterns observed here are specific to equation (3), the notion that such patterns dominate the structure of/is, probably, much more general, and should be pursued as a systematic road map for analysing complex system dynamics.

Online content

Any methods, additional references, Nature Portfolio reporting summaries, source data, extended data, supplementary information, acknowledgements, peer review information; details of author contributions and competing interests; and statements of data and code availability are available at <https://doi.org/10.1038/s41567-023-02020-8>.

References

- Buldyrev, S. V., Parshani, R., Paul, G., Stanley, H. E. & Havlin, S. Catastrophic cascade of failures in interdependent networks. *Nature* **464**, 1025–1028 (2010).
- Dobson, I., Carreras, B. A., Lynch, V. E. & Newman, D. E. Complex systems analysis of series of blackouts: cascading failure, critical points, and self-organization. *Chaos* **17**, 026103 (2007).
- Duan, D. et al. Universal behavior of cascading failures in interdependent networks. *Proc. Natl Acad. Sci. USA* **116**, 22452–22457 (2019).
- Motter, A. E. & Lai, Y.-C. Cascade-based attacks on complex networks. *Phys. Rev. E* **66**, 065102 (2002).
- Crucitti, P., Latora, V. & Marchiori, M. Model for cascading failures in complex networks. *Phys. Rev. E* **69**, 045104 (2004).
- Achlioptas, D., D'Souza, R. M. & Spencer, J. Explosive percolation in random networks. *Science* **323**, 1453–1455 (2009).
- Gao, J., Barzel, B. & Barabási, A.-L. Universal resilience patterns in complex networks. *Nature* **530**, 307–312 (2016).
- Boccaletti, S. et al. Explosive transitions in complex networks' structure and dynamics: percolation and synchronization. *Phys. Rep.* **660**, 1–94 (2016).
- Boccaletti, S., Latora, V., Moreno, Y., Chavez, M. & Hwang, D.-U. Complex networks: structure and dynamics. *Phys. Rep.* **424**, 175–308 (2006).
- Danziger, M. M., Bonamassa, Ivan, Boccaletti, Stefano & Havlin, Shlomo Dynamic interdependence and competition in multilayer networks. *Nat. Phys.* **15**, 178–185 (2019).
- Coyte, K. Z., Schlüter, J. & Foster, K. R. The ecology of the microbiome: networks, competition, and stability. *Science* **350**, 663–666 (2015).
- Solé, R. V. & Montoya, J. M. Complexity and fragility in ecological networks. *Proc. R. Soc. Lond. B* **268**, 2039–2045 (2001).
- Schreier, H. I., Soen, Y. & Brenner, N. Exploratory adaptation in large random networks. *Nat. Commun.* **8**, 14826 (2017).
- Pecora, L. M. & Carroll, T. L. Master stability functions for synchronized coupled systems. *Phys. Rev. Lett.* **80**, 2109 (1998).
- Arnold, V. I. *Ordinary Differential Equations* (MIT Press, 1973).
- Hirsch, M. W. & Smale, S. *Differential Equations, Dynamical Systems and Linear Algebra* (Academic Press, 1974).
- McCann, K. S. The diversity–stability debate. *Nature* **405**, 228–233 (2000).
- O'Sullivan, J. D., Knell, R. J. & Rossberg, A. G. Metacommunity-scale biodiversity regulation and the self-organised emergence of macroecological patterns. *Ecol. Lett.* **22**, 1428–1438 (2019).
- Barbier, M., de Mazancourt, C., Loreau, M. & Bunin, G. Fingerprints of high-dimensional coexistence in complex ecosystems. *Phys. Rev. X* **11**, 011009 (2021).
- Caldarelli, G. *Scale-Free Networks: Complex Webs in Nature and Technology* (Oxford Univ. Press, 2007).
- May, R. M. Will a large complex system be stable? *Nature* **238**, 413–414 (1972).
- Barzel, B. & Barabási, A.-L. Universality in network dynamics. *Nat. Phys.* **9**, 673–681 (2013).
- Harush, U. & Barzel, B. Dynamic patterns of information flow in complex networks. *Nat. Commun.* **8**, 2181 (2017).
- Hens, C., Harush, U., Cohen, R., Haber, S. & Barzel, B. Spatiotemporal propagation of signals in complex networks. *Nat. Phys.* **15**, 403–412 (2019).
- Pastor-Satorras, R., Castellano, C., Van Mieghem, P. & Vespignani, A. Epidemic processes in complex networks. *Rev. Mod. Phys.* **87**, 925–958 (2015).
- Dodds, P. S., Muhamad, R. & Watts, D. J. An experimental study of search in global social networks. *Science* **301**, 827–829 (2003).
- Brockmann, D., David, V. & Gallardo, A. M. Human mobility and spatial disease dynamics. *Rev. Nonlinear Dyn. Complex.* **2**, 1 (2009).
- Karlebach, G. & Shamir, R. Modelling and analysis of gene regulatory networks. *Nat. Rev.* **9**, 770–780 (2008).
- Murray, J. D. *Mathematical Biology* (Springer, 1989).
- Barzel, B. & Biham, O. Binomial moment equations for stochastic reaction systems. *Phys. Rev. Lett.* **106**, 150602 (2011).

31. Barzel, B. & Biham, O. Stochastic analysis of complex reaction networks using binomial moment equations. *Phys. Rev. E* **86**, 031126 (2012).
32. Holling, C. S. Some characteristics of simple types of predation and parasitism. *Can. Entomol.* **91**, 385–398 (1959).
33. Holland, J. N., DeAngelis, D. L. & Bronstein, J. L. Population dynamics and mutualism: functional responses of benefits and costs. *Am. Nat.* **159**, 231–244 (2002).
34. Wodarz, D., Christensen, J. P. & Thomsen, A. R. The importance of lytic and nonlytic immune responses in viral infections. *Trends Immunol.* **23**, 194–200 (2002).
35. Berlow, E. L. et al. Simple prediction of interaction strengths in complex food webs. *Proc. Natl Acad. Sci. USA* **106**, 187–191 (2009).
36. Hayes, J. F. & Ganesh Babu, T. V. J. *Modeling and Analysis of Telecommunications Networks* (John Wiley & Sons, 2004).
37. Newman, M. E. J. *Networks—An Introduction* (Oxford Univ. Press, 2010).
38. Yan, G., Martinez, N. D. & Liu, Y.-Y. Degree heterogeneity and stability of ecological networks. *J. R. Soc. Interface* **14**, 20170189 (2017).
39. Almendral, J. A. & Díaz-Guilera, A. Dynamical and spectral properties of complex networks. *New J. Phys.* **9**, 187 (2007).
40. Van Mieghem, P. Epidemic phase transition of the SIS type in network. *Europhys. Lett.* **97**, 48004 (2012).
41. Van Mieghem, P. *Graph Spectra for Complex Networks* (Cambridge Univ. Press, 2010).
42. Milojević, S. Power-law distributions in information science: making the case for logarithmic binning. *J. Am. Soc. Inf. Sci. Technol.* **61**, 2417–2425 (2010).
43. Allesina, S. & Tang, S. Stability criteria for complex ecosystems. *Nature* **483**, 205–208 (2012).
44. Tarnowski, W., Neri, I. & Vivo, P. Universal transient behavior in large dynamical systems on networks. *Phys. Rev. Research* **2**, 023333 (2020).
45. Sinha, S. & Sinha, S. Evidence of universality for the May-Wigner stability theorem for random networks with local dynamics. *Phys. Rev. E* **71**, 020902 (2005).
46. Kirk, P., Rolando, D. M. Y., MacLean, A. L. & Stumpf, M. P. H. Conditional random matrix ensembles and the stability of dynamical systems. *New J. Phys.* **17**, 080325 (2015).

Publisher's note Springer Nature remains neutral with regard to jurisdictional claims in published maps and institutional affiliations.

Springer Nature or its licensor (e.g. a society or other partner) holds exclusive rights to this article under a publishing agreement with the author(s) or other rightsholder(s); author self-archiving of the accepted manuscript version of this article is solely governed by the terms of such publishing agreement and applicable law.

© The Author(s), under exclusive licence to Springer Nature Limited 2023

Methods

Random-matrix-based Jacobian constructions

The random matrix paradigm was first introduced by May²¹, precisely seeking the question we address here (Fig. 5): will a large complex system be stable? In this original construction, all the diagonal weights in equation (2) were set to $W_{ii} = 1$, whereas the off-diagonal weights were extracted from a zero-mean Gaussian distribution. The rationale is that the self-regulation of all the components is uniform, driven by the system's intrinsic timescales (normalized to unity), whereas the interaction strengths randomly vary around zero. Such a construction is a particular case of our W_{ii} in equation (4), setting $C(\mathbf{f}, \mathbf{g}) = 1$ and $\eta = \mu = 0$. Although May's first assumption about $C(\mathbf{f}, \mathbf{g})$ has no significant bearing on our analysis, his second assumption, which ignores the dynamic exponents η and μ , is precisely the crux of our proposed novelty. Indeed, in our framework, it is these two exponents (together with v and ρ) that capture the role of the nonlinear dynamics, a role that is ignored in the random matrix constructions.

In the works that followed May's abstract construction, researchers systematically introduced more realism into J . First, more realistic A_{ij} were considered, for example, small-world⁴⁷ or scale-free networks³⁸, which have, indeed, been shown to impact the spectral properties of equation (2). Other advances tackled $P_0(w)$ and $P_1(w)$, showing that different dynamics may lead to more specific weight distributions, rather than the originally assumed Gaussian distribution. This is achieved by conditioning $P_0(w)$ and $P_1(w)$ to account for specific patterns that arise from known dynamic processes. For example, in predator-prey relationships, a positive W_{ij} is often matched with a negative W_{ji} (refs. 43,44), capturing the asymmetry in the benefit/loss of the predator and its prey. More complex dynamic constraints may further impact the statistical properties of W , limiting the Jacobian to a selected subset of the random matrix ensemble⁴⁶.

Deriving the dynamic Jacobian ensemble

Although we provide a complete and rigorous derivation of the $\mathbb{E}(A, G, \Omega)$ ensemble (Supplementary Sections 1–3), below we include a shorthand version of this derivation, tracking the main steps and important mathematical transitions leading to equations (4), (5) and (9). For simplicity, in this abbreviated analysis, we limit ourselves to systems with uniform weights/parameters. Hence, in equation (3), we set the global and individual weights to $g = G_{ij} = 1$ and take $\mathbf{f}_{qi} = \mathbf{f}_{qj}$ for all $i, j = 1, \dots, N$. Under these simplifications, we rewrite equation (3) as

$$\frac{dx_i}{dt} = M_0(x_i(t)) + M_1(x_i(t)) \sum_{j=1}^N A_{ij} M_2(x_j(t)), \quad (11)$$

omitting the link weights g, G_{ij} and parameters \mathbf{f}_{qi} , which are now identical for all the nodes. We emphasize that in our full derivation, as well as in our reported results and simulations, we do not rely on these simplified assumptions, and only employ them here for brevity and conciseness.

Fixed-point analysis. Starting from equation (11), we seek the system's potential fixed points via

$$M_0(x_i) + M_1(x_i) \sum_{j=1}^N A_{ij} M_2(x_j) = 0, \quad (12)$$

where we use x_i (omitting the t dependence) to denote the fixed point $x_i = x_i(t \rightarrow \infty)$. To express the summation over j in the left-hand side, we use

$$\langle M_2(x) \rangle_{i\odot} = \frac{1}{d_i} \sum_{j=1}^N A_{ij} M_2(x_j), \quad (13)$$

capturing a weighted average over $M_2(x_j)$ across all the nearest neighbours of i . Here, with all the link weights set to unity, $d_i = \sum_{j=1}^N A_{ij}$ represents the binary degree of i . This generalizes to the weighted degree of i if we reintroduce our weights g and G_{ij} . In equation (13), we use the notation \odot to represent a neighbourhood average, namely, an average over the surrounding nodes of i , namely, $i\odot$. Substituting equation (13) into equation (12), we obtain

$$M_0(x_i) + d_i M_1(x_i) \langle M_2(x) \rangle_{i\odot} = 0, \quad (14)$$

which we further simplify to

$$R(x_i) = q_i \quad (15)$$

where $R(x) = -M_1(x)/M_0(x)$ and

$$q_i = \frac{1}{\langle M_2(x) \rangle_{i\odot} d_i} \quad (16)$$

is the inverse weighted degree of node i . In equation (15), the function $R(x)$ is only defined in case $M_0(x) \neq 0$. The treatment of $M_0(x) = 0$ is separately provided (Supplementary Section 2.5). We can now extract the fixed point x_i by inverting $R(x_i)$ to obtain

$$x_i = R^{-1}(q_i), \quad (17)$$

allowing us to express the fixed-point activity of node i in function of its inverse degree q_i . Here we rely on the implicit assumption that $R(x)$ is invertible, allowing us to write $R^{-1}(q)$ in equation (17). As above, we employ this assumption here only for simplicity; in our complete derivation (Supplementary Section 2), we show how to obtain x_i even under non-invertible $R(x)$.

Jacobian scaling—diagonal weights W_{ii} . We now return to equation (11) to extract the Jacobian weights W_{ii} and W_{ij} around the fixed point obtained in equation (17). Starting with the diagonal terms, we write

$$W_{ii} = \left. \frac{\partial \dot{x}_i}{\partial x_i} \right|_{x_i=R^{-1}(q_i)} = \left. \left(M'_0(x_i) + M'_1(x_i) \sum_{j=1}^N A_{ij} M_2(x_j) \right) \right|_{x_i=R^{-1}(q_i)}, \quad (18)$$

where $M'_q(x) = \partial M_q/\partial x$. Equation (18) represents a derivative of the right-hand side of equation (11) taken around the fixed point x_i , which we express via equation (17) as $R^{-1}(q_i)$. Next, we use $R(x) = -M_1(x)/M_0(x)$ to write $M_0(x) = -M_1(x)/R(x)$, allowing us to express the first derivative on the right-hand side of equation (18) as

$$M'_0(x_i) = -\frac{M'_1(x_i)}{R(x_i)} + \frac{M_1(x_i) R'(x_i)}{R^2(x_i)}, \quad (19)$$

which, setting $x_i = R^{-1}(q_i)$, provides

$$M'_0(x) = -\frac{M'_1(R^{-1}(q_i))}{q_i} + \frac{M_1(R^{-1}(q_i)) R'(R^{-1}(q_i))}{q_i^2}. \quad (20)$$

To obtain the denominators q_i and q_i^2 above, we used the fact that $R(R^{-1}(q_i)) = q_i$. We can now use equation (13) to express the sum on the right-hand side of equation (18) as $\sum_{j=1}^N A_{ij} M_2(x_j) = d_i \langle M_2(x) \rangle_{i\odot}$, which, according to equation (16), is equal to $1/q_i$. Collecting all the terms, we arrive at

$$W_{ii} = -\frac{M'_1(R^{-1}(q_i))}{q_i} + \frac{M_1(R^{-1}(q_i)) R'(R^{-1}(q_i))}{q_i^2} + \frac{M'_1(R^{-1}(q_i))}{q_i}, \quad (21)$$

which, in turn, provides

$$W_{ii} = \frac{1}{q_i^2} Y(R^{-1}(q_i)), \quad (22)$$

where $Y(x) = M_1(x)R'(x)$.

Equation (22) expresses the diagonal Jacobian weight W_{ii} in terms of the inverse degree of i , $q_i \sim d_i^{-1}$. In the asymptotic limit of large d_i (small q_i), we can approximate equation (22) by expanding $Y(R^{-1}(q_i))$ around $q_i = 0$. We, therefore, express this function as a Hahn⁴⁸ power series expansion in the form

$$Y(R^{-1}(q_i)) = \sum_{n=0}^{\infty} B_n q_i^{\phi_n}, \quad (23)$$

allowing us to examine the limit $q_i \rightarrow 0$ below. The Hahn series in equation (23) represents a generalization of the Taylor expansion to allow for negative and real powers; hence, $\phi_n \in \mathbb{R}$ captures a sequence of real powers in ascending order, that is, $\phi_0 < \phi_1$ and so on. In the limit $q_i \rightarrow 0$, we take only the leading term $q_i^{\phi_0}$, which, in equation (22), provides the scaling relationship

$$W_{ii} \sim B_0 q_i^{-\mu} = B_0 (\langle M_2(x) \rangle_{i\odot} d_i)^{\mu}, \quad (24)$$

where $\mu = 2 - \phi_0$. In the last step of equation (24), we reintroduced d_i using the definition of q_i in equation (16), thereby also adding the neighbourhood average of i , $\langle M_2(x) \rangle_{i\odot}$.

Equation (24) describes the weight of the diagonal Jacobian entry associated with a specific node i . It is found to not only depend on the node's degree d_i but also on the activity of its neighbouring nodes via $\langle M_2(x) \rangle_{i\odot}$. To complete the scaling of W_{ii} with d_i , we must characterize the d_i dependence of $\langle M_2(x) \rangle_{i\odot}$. The crucial point is that $\langle M_2(x) \rangle_{i\odot}$ captures an average over the neighbourhood of i , not over the node i itself, and hence, on average, it is only indirectly affected by d_i . To express this more rigorously, we write

$$\langle M_2(x) \rangle_{i\odot} \sim \langle M_2(x) \rangle_{\odot} f(d_i), \quad (25)$$

replacing the average over the neighbourhood of i ($i\odot$) with the ensemble average (\odot). This ensemble average $\langle M_2(x) \rangle_{\odot} = (1/N) \sum_{i=1}^N \langle M_2(x) \rangle_{i\odot}$ represents an aggregation over all the nodes in the network, and hence, it is independent of i or d_i . To account for the potential d_i dependence, we include, on the right-hand side of equation (25), the implicit function $f(d_i)$. This function, defined as $f(d_i) = \langle M_2(x) \rangle_{i\odot} / \langle M_2(x) \rangle_{\odot}$, captures the distinction between the conditional i -neighbourhood average ($i\odot$) and the network's ensemble average (\odot). It, therefore, helps quantify potential statistical dependencies between i and its interacting neighbours $i\odot$. Hence, if the network is randomly wired, that is, lacks degree correlations³⁷, we have $f(d_i) = 1$, independent of i . However, if correlations are present, it will be expressed through a non-trivial $f(d_i)$.

Extracting only the terms that depend on d_i , we rewrite equation (24) as $W_{ii} \sim f(d_i) d_i^{\mu}$, omitting the terms B_0 and $\langle M_2(x) \rangle_{\odot}$, which are independent of d_i . Finally, if $f(d_i)$ is subpolynomial, it does not contribute to d_i scaling in the limit of large d_i . This allows us to write

$$W_{ii} \sim d_i^{\mu}, \quad (26)$$

recovering the asymptotic scaling relationship of equation (4). In equation (26), we eliminated all the terms that do not contribute to the polynomial dependence on d_i , thus solely focusing on the obtained scaling relationship. These terms may, however, depend on other parameters of equation (3). For example, fairly expectedly, the term $\langle M_2(x) \rangle_{\odot}$, an average driven by the activity of all the nearest-neighbour nodes is potentially dependent on the nearest-neighbour degree d_{nn} in equation (6). Similarly, the coefficient B_0 is, most often, a function

of parameters \mathbf{f} and g in equation (3). These additional dependencies are precisely what gives rise to the prefactors $C(\mathbf{f}, g) d_{nn}^{\eta}$ in equation (4), which we ignored in the present derivation (Supplementary Section 2 provides the complete derivation, which also covers these terms).

The substitution leading to equations (25) and (26) represents our first approximation, where we assume that $\langle M_2(x) \rangle_{i\odot}$ is only weakly dependent on d_i . This weak dependence is precisely defined by the assumption that $f(d_i)$ is subpolynomial, for example, $f(d_i) \approx \log d_i$. This implies that the neighbours of node i with degree d_i are—to a sufficient degree—statistically similar to those of j whose degree is d_j . Under this approximation, averaging over a node's neighbourhood, conditional on that node's degree (as done in the right-hand side of equation (24)), is (almost) the same as averaging over the neighbours of any other node, independent of degree (indeed, up to the subpolynomial correction $f(d_i)$). In Supplementary Section 1.2, we elaborate on the relevance of this approximation, and in Supplementary Fig. 2, we explicitly measure $f(d_i)$ for our entire testing ground of networks/dynamics. We find that $f(d_i)$ is, indeed, at most logarithmic, supporting the relevance of our approximation for our set of real/model networks.

Off-diagonal weights W_{ij} . To extract the off-diagonal terms $i \neq j$ of $\mathbb{E}(A, G, \Omega)$, we return to equation (11), this time writing

$$W_{ij} = \left. \frac{\partial x_i}{\partial x_j} \right|_{x_i = R^{-1}(q_i)} = \left. \frac{\partial}{\partial x_j} \left(M_0(x_i) + M_1(x_i) \sum_{n=1}^N A_{in} M_2(x_n) \right) \right|_{x_i = R^{-1}(q_i)} \quad (27)$$

$$x_j = R^{-1}(q_j) \quad x_j = R^{-1}(q_j)$$

Keeping only the terms that explicitly depend on x_j , we obtain

$$W_{ij} = M_1(x_i) A_{ij} M'_2(x_j) \Big|_{x_i = R^{-1}(q_i)} = M_1(R^{-1}(q_i)) A_{ij} M'_2(R^{-1}(q_j)), \quad (28)$$

$$x_j = R^{-1}(q_j)$$

helping us identify the two relevant dynamic functions $M_1(R^{-1}(q_i))$ and $M'_2(R^{-1}(q_j))$, whose leading powers determine the scaling of W_{ij} . Expressing these functions as a Hahn series, we write

$$M_1(R^{-1}(q_i)) = \sum_{n=0}^{\infty} K_n q_i^{\pi_n}, \quad (29)$$

$$M'_2(R^{-1}(q_j)) = \sum_{n=0}^{\infty} L_n q_j^{\phi_n}, \quad (30)$$

and in the limit of large d_i and d_j (small q_i and q_j) take only the leading terms, namely, $\sim q_i^{\pi_0}$ and $\sim q_j^{\phi_0}$, respectively. Substituting these terms into equation (28), and using the fact that $q_i \sim d_i^{-1}$, we arrive at

$$W_{ij} \sim d_i^{\nu} A_{ij} d_j^{\rho}, \quad (31)$$

where $\nu = -\pi_0$ and $\rho = -\phi_0$, recovering the prediction of equation (5), under the current setting of $G_{ij} = 1$, that is, unweighted.

The obtained exponents μ , ν and ρ are extracted from the leading powers of our derived dynamic functions $Y(R^{-1}(x))$ in equation (23), $M_1(R^{-1}(x))$ in equation (29) and $M'_2(R^{-1}(x))$ in equation (30). These functions, in turn, are directly linked to $M_n(x)$ in equation (3) and hence offer a direct procedure by which to extract the $\mathbb{E}(A, G, \Omega)$ Jacobian scaling relationships (Fig. 1). The fourth and final exponent η in equation (4) can be extracted in a similar fashion (Supplementary Section 2).

Practical summary—calculating Ω

Although the derivation in the ‘Deriving the dynamic Jacobian ensemble’ section may be elaborate, its practical outcome is rather straightforward, providing a step-by-step recipe by which the exponent set $\Omega = (\eta, \mu, \nu, \rho)$ in equations (4) and (5) can be constructed. First, we use

the dynamic functions $M_0(x)$, $M_1(x)$ and $M_2(x)$ (equation (3)) to construct the three secondary functions:

$$R(x) = -\frac{M_1(x)}{M_0(x)}, \quad Y(x) = M_1(x)R'(x), \quad Z(x) = R(x)M_2(x). \quad (32)$$

The functions $R(x)$ and $Y(x)$ are introduced in the ‘Deriving the dynamic Jacobian ensemble’ section; Supplementary Section 2 provides the derivation of $Z(x)$. From equation (32), we extract four additional functions, which we express through a Hahn power series expansion as

$$M_2(Z^{-1}(x)) = \sum_{n=0}^{\infty} G_n x^{\Psi_n}, \quad Y(R^{-1}(x)) = \sum_{n=0}^{\infty} C_n x^{\Phi_n}, \quad (33)$$

$$M_1(R^{-1}(x)) = \sum_{n=0}^{\infty} K_n x^{\Pi_n}, \quad M'_2(R^{-1}(x)) = \sum_{n=0}^{\infty} L_n x^{\Theta_n}.$$

We use $R^{-1}(x)$ and $Z^{-1}(x)$ to denote the inverse functions of $R(x)$ and $Z(x)$, respectively. The leading powers ($n = 0$) in these Hahn series directly provide Ω via

$$\mu = 2 - \Phi_0, \quad \nu = -\Pi_0, \quad \rho = -\Theta_0, \quad \eta = -\Psi_0(\mu - \nu - \rho). \quad (34)$$

Hence, to construct $J \in \mathbb{E}(A, G, \Omega)$, we first generate the weighted network $A \circ G$ and then extract the weighted degrees d_i and d_j of all the nodes and the nearest-neighbour degree d_{nn} (equation (6)). The resulting J satisfies

$$J_{ii} \sim -C(f, g)d_{nn}^{\eta} d_i^{\mu}, \quad (35)$$

$$J_{ij} \sim d_i^{\nu} A_{ij} G_{ij} d_j^{\rho}, \quad (36)$$

where the coefficient $C(f, g) > 0$ encapsulates the system’s specific rate parameters (we do not attempt to predict this coefficient in the current formalism). Supplementary Section 2 provides a detailed derivation of Ω followed by a step-by-step application on all our testing ground dynamics (Fig. 2 and Supplementary Section 4).

In the above formulation, we have assumed that $R(x)$ and $Z(x)$ are invertible, writing $R^{-1}(x)$ and $Z^{-1}(x)$ in equation (33), respectively. Supplementary Section 2 explains how to properly treat non-invertible $R(x)$ and $Z(x)$. In these sections, we also demonstrate how to extract J for systems with multiple fixed points; finally, Supplementary Section 2.5 shows how to construct J around a trivial fixed point $\mathbf{x} = (0, \dots, 0)^T$.

Ingredients of $\mathbb{E}(A, G, \Omega)$

In equation (3), we distinguish between the nonlinear form of the functions $M_q(x)$ and their specific parameters \mathbf{f}_{qi} . The former, we argue, is designed to mathematically represent the nodes’ intrinsic driving mechanisms, for example, distinguishing between Epidemic and Biochemical dynamics. The latter, on the other hand, describes the specific rates of these mechanistic processes, which may potentially change across nodes/links or under different environmental conditions. To root this distinction on mathematical grounds, we refer again to the Hahn expansion, and express each of the functions $M_q(x, \mathbf{f}_{qi})$ via

$$M_q(x_i, \mathbf{f}_{qi}) = \sum_{n=0}^{\infty} C_{qn}(\mathbf{f}_{qi}) x_i^{\Gamma_{qn}}. \quad (37)$$

In equation (37), we distinguish between the role of powers Γ_{qn} and that of coefficients C_{qn} . The powers, in most cases, characterize the functional form of $M_q(x, \mathbf{f}_{qi})$, differentiating, for example, between $M_q(x, \mathbf{f}_{qi}) \sim x^2$ and $M_q(x, \mathbf{f}_{qi}) \sim x/(1+x)$. These different functions are designed to mathematically represent distinct microscopic

mechanisms, for example, social interactions versus biological processes. As these mechanisms are ingrained into the physics of the interacting components, we take them, in our formulation, to be fixed and uniform across all nodes/links. In contrast, the coefficients C_{qn} are often tunable, depending on the particular rates characterizing each node’s dynamics, and hence, they depend on the node-specific parameters \mathbf{f}_{qi} .

To better understand this distinction, let us consider a specific example of logistic growth, a common mechanism in population dynamics. Within the dynamic framework of equation (3), this mechanism is captured by $M_0(x_i) = b_i x_i(1 - x_i/c_i)$, which, written in the form of equation (37), provides $M_0(x_i) = b_i x_i - (b_i/c_i)x_i^2$. Namely, the coefficients are $C_{00} = b_i$ and $C_{01} = -b_i/c_i$, and the corresponding powers are $\Gamma_{00} = 1$ and $\Gamma_{01} = 2$. The crucial point is that while b_i and c_i , that is, the species growth rate and the system’s carrying capacity, respectively, are node dependent and potentially affected by environmental conditions, the functional form $M_q(x_i) \sim x_i(1 - x_i)$ is intrinsic to logistic growth and cannot be easily perturbed. This is precisely captured by the separate role of powers versus coefficients: the tunable parameters b_i and c_i are expressed only within C_{qn} , whereas the functional form of logistic growth is embedded within the powers Γ_{qn} —here describing linear growth ($\Gamma_{00} = 1$) followed by quadratic attenuation due to intraspecies competition ($\Gamma_{01} = 2$).

Hence, from a strictly mathematical perspective, we define parameters as the factors affecting coefficients C_{qn} in equation (37), and functional form via the set of participating powers Γ_{qn} . Our interpretation of this mathematical distinction is that the powers are more intrinsic than coefficients. Indeed, in our logistic growth example, the two powers arise from the system’s ingrained driving mechanisms—growth (linear) versus competition (quadratic). In contrast, the coefficients depend on parameters b_i and c_i , which may assume any value within the logistic growth framework, and can even change due to external conditions.

The crucial point is that our Jacobian scaling exponents Ω depend only on powers Γ_{qn} and are unrelated to coefficients C_{qn} . Hence, in our example, all the systems driven by logistic growth (and a matching interaction dynamics) will have similar Ω , regardless of the specific parameters b_i and c_i . This portrays Ω and its resulting S as innate built-in characteristics of the system’s dynamics, detached from its multitude of microscopic parameters. Consequently, our asymptotic stable/unstable classes are intrinsic to the system’s dynamics, insensitive to external perturbation or to microscopic discrepancies.

Generality and limitations of the $\mathbb{E}(A, G, \Omega)$ ensemble

Dynamic limitations. Our ensemble $\mathbb{E}(A, G, \Omega)$ was analytically derived under the conditions defined by equation (3). Despite its general structure, we wish to emphasize that this equation still excludes several families of dynamics, for example, non-additive interactions or threshold models.⁴⁹ Similarly, if the system incorporates a mixture of distinct interaction mechanisms, such that every node/link is driven by its own idiosyncratic processes, the dynamics cannot be cast into the form $M_0(x), M_1(x), M_2(x)$.

We note, however, that although our analytical derivations are, indeed, bounded by these restrictions, the family of potential dynamics included within the $\mathbb{E}(A, G, \Omega)$ ensemble may, in fact, be broader. Specifically, we consider (Supplementary Section 5) several expansions to equation (3) that help us examine the applicability limits of our dynamic Jacobians.

- Non-factorizable interactions.** Our testing ground includes power dynamics, in which the interaction term cannot be partitioned into a product $M_1(x_i)M_2(x_j)$, but rather incorporates a diffusive mechanism of the form $M(x_i - x_j)$. Such dynamics, excluded from equation (3), arise in different contexts, from reaction–diffusion to synchronization^{50,51}, and despite the fact that they are not covered by our analytical framework, our analysis of power indicates that they continue to fall within $\mathbb{E}(A, G, \Omega)$.

- **Non-additive interactions.** Another outlier in Fig. 2 is Population 2, in which the linear sum $\sum_{j=1}^N M_2(x_j)$ is replaced by $M_2(\sum_{j=1}^N x_j)$, again—outside the bounds of equation (3). Still, as shown, for example, in Fig. 3n,o, this system also has $J \in \mathbb{E}(A, G, \Omega)$.
- **Mixed dynamics.** The last assumption we challenge is the notion that all the components are driven by similar dynamic processes, as expressed by the uniform functional form of $M_q(x)$ across all the nodes. In Supplementary Sections 5.4 and 5.5, we numerically examine systems with two or three competing self-dynamics or interaction dynamics. We find that the Jacobians of such systems exhibit coexisting scaling relationships with exponent sets $\Omega_1, \Omega_2, \dots$, corresponding to the network's distinct dynamic mechanisms. This captures a natural generalization of $\mathbb{E}(A, G, \Omega)$, which indicates the potential qualitative insights offered by our analysis, even beyond the technical limits of equation (3).

Topological limitations

Our predicted asymptotic stability/instability is driven by the limit of large d , that is, the hubs. It is, therefore, mainly relevant for degree-heterogeneous networks. Although extreme heterogeneity is, indeed, common in many biological and social systems, there are areas, such as ecological systems⁵², where the networks tend to be more homogeneous. Under such conditions, our theory predicts that the system is in the sensitive class: it could be stable, but its stability is not guaranteed in the face of parameter perturbation.

Finally, our asymptotic predictions capture the system's global stability, but have no bearing on the dynamic stability of small motifs or subnetworks, which may be locally unstable. Still, in an asymptotically stable system, the global impact of such unstable motifs vanishes in the limit of large N , and hence, the system as a whole remains insensitive to these local discrepancies. Supplementary Section 6 discusses this in detail, including extensive numerical support.

Data availability

All empirical network data to retrieve the results shown here are available via GitLab at https://gitlab.com/meenachandrakala/Dynamic_Stability/-/tree/master/Dynamic_Stability.

Code availability

All code to reproduce the results shown here is available via GitLab at https://gitlab.com/meenachandrakala/Dynamic_Stability/-/tree/master/Dynamic_Stability.

References

47. Watts, D. J. & Strogatz, S. H. Collective dynamics of 'small-world' networks. *Nature* **393**, 440–442 (1998).
48. Schmetterer, L. & Sigmund, K. (eds) *Hans Hahn Gesammelte Abhandlungen Band 1/Hans Hahn Collected Works Volume 1* (Springer, 1995).
49. Granovetter, M. Threshold models of collective behavior. *Am. J. Sociol.* **83**, 1420–1443 (2002).
50. Kuramoto, Y. *Chemical Oscillations, Waves and Turbulence* (Springer, 1984).
51. Kundu, P., Hens, C., Barzel, B. & Pal, P. Perfect synchronization in networks of phase-frustrated oscillators. *Europhys. Lett.* **120**, 40002 (2018).
52. Stouffer, D. B., Camacho, J., Guimerà, R., Ng, C. A. & Nunes Amaral, L. A. Quantitative patterns in the structure of model and empirical food webs. *Ecology* **86**, 1301–1311 (2005).

Acknowledgements

This work is dedicated in memory of Robert May. We wish to thank I. Conforti for designing inspiring artwork to accompany our scientific research. C.M. thanks the Planning and Budgeting Committee (PBC) of the Council for Higher Education, Israel, for support. C.M. is also supported by the INSPIRE-Faculty grant (code IFA19-PH248) of the Department of Science and Technology, India. C.H. is supported by the INSPIRE-Faculty grant (code IFA17-PH193) of the Department of Science and Technology, India. S.H. has contributed to this work while visiting the mathematics department of Rutgers University, New Brunswick. S.B. acknowledges funding from the project EXPLICS granted by the Italian Ministry of Foreign Affairs and International Cooperation. This research was also supported by the Israel Science Foundation (grant no. 499/19), the Israel-China ISF-NSFC joint research program (grant no. 3552/21), the US National Science Foundation CRISP award no. 1735505, and by the Bar-Ilan University Data Science Institute grant for data science research. In memory of Robert May.

Author contributions

All authors designed and planned the research and derived the analytical results. C.M., with the aid of C.H. and S.A., conducted the data analysis and numerical simulations. B.B. was the lead writer of the paper.

Competing interests

The authors declare no competing interests.

Additional information

Supplementary information The online version contains supplementary material available at <https://doi.org/10.1038/s41567-023-02020-8>.

Correspondence and requests for materials should be addressed to Chandrakala Meena or Baruch Barzel.

Peer review information *Nature Physics* thanks Axel Rossberg, Neo Martinez and Jobst Heitzig for their contribution to the peer review of this work.

Reprints and permissions information is available at www.nature.com/reprints.

Terms and Conditions

Springer Nature journal content, brought to you courtesy of Springer Nature Customer Service Center GmbH (“Springer Nature”). Springer Nature supports a reasonable amount of sharing of research papers by authors, subscribers and authorised users (“Users”), for small-scale personal, non-commercial use provided that all copyright, trade and service marks and other proprietary notices are maintained. By accessing, sharing, receiving or otherwise using the Springer Nature journal content you agree to these terms of use (“Terms”). For these purposes, Springer Nature considers academic use (by researchers and students) to be non-commercial.

These Terms are supplementary and will apply in addition to any applicable website terms and conditions, a relevant site licence or a personal subscription. These Terms will prevail over any conflict or ambiguity with regards to the relevant terms, a site licence or a personal subscription (to the extent of the conflict or ambiguity only). For Creative Commons-licensed articles, the terms of the Creative Commons license used will apply.

We collect and use personal data to provide access to the Springer Nature journal content. We may also use these personal data internally within ResearchGate and Springer Nature and as agreed share it, in an anonymised way, for purposes of tracking, analysis and reporting. We will not otherwise disclose your personal data outside the ResearchGate or the Springer Nature group of companies unless we have your permission as detailed in the Privacy Policy.

While Users may use the Springer Nature journal content for small scale, personal non-commercial use, it is important to note that Users may not:

1. use such content for the purpose of providing other users with access on a regular or large scale basis or as a means to circumvent access control;
2. use such content where to do so would be considered a criminal or statutory offence in any jurisdiction, or gives rise to civil liability, or is otherwise unlawful;
3. falsely or misleadingly imply or suggest endorsement, approval , sponsorship, or association unless explicitly agreed to by Springer Nature in writing;
4. use bots or other automated methods to access the content or redirect messages
5. override any security feature or exclusionary protocol; or
6. share the content in order to create substitute for Springer Nature products or services or a systematic database of Springer Nature journal content.

In line with the restriction against commercial use, Springer Nature does not permit the creation of a product or service that creates revenue, royalties, rent or income from our content or its inclusion as part of a paid for service or for other commercial gain. Springer Nature journal content cannot be used for inter-library loans and librarians may not upload Springer Nature journal content on a large scale into their, or any other, institutional repository.

These terms of use are reviewed regularly and may be amended at any time. Springer Nature is not obligated to publish any information or content on this website and may remove it or features or functionality at our sole discretion, at any time with or without notice. Springer Nature may revoke this licence to you at any time and remove access to any copies of the Springer Nature journal content which have been saved.

To the fullest extent permitted by law, Springer Nature makes no warranties, representations or guarantees to Users, either express or implied with respect to the Springer nature journal content and all parties disclaim and waive any implied warranties or warranties imposed by law, including merchantability or fitness for any particular purpose.

Please note that these rights do not automatically extend to content, data or other material published by Springer Nature that may be licensed from third parties.

If you would like to use or distribute our Springer Nature journal content to a wider audience or on a regular basis or in any other manner not expressly permitted by these Terms, please contact Springer Nature at

onlineservice@springernature.com